Mineralogy and Petrology (2020) 114:443–451
https://doi.org/10.1007/s00710-020-00703-1

ORIGINAL PAPER

Roterbärite, $PdCuBiSe_3$, a new mineral species from the Roter Bär mine, Harz Mountains, Germany

Anna Vymazalová[1] · Alexandre R. Cabral[2,3] · František Laufek[1] · Wilfried Ließmann[4] · Chris J. Stanley[5] · Bernd Lehmann[4]

Received: 26 October 2019 / Accepted: 3 March 2020 / Published online: 4 June 2020

Abstract

Roterbärite, $PdCuBiSe_3$, is a new mineral species from the Roter Bär mine, Harz Mountains, Germany. It forms euhedral to subhedral grains, up to 50 μm across, embedded in clausthalite, which is spatially associated with gold, mertieite-II, bohdanowiczite, hematite, chalcopyrite, baryte, ankerite and dolomite. Roterbärite is brittle and has a metallic luster. In plane-polarized light, roterbärite is slightly pleochroic in shades of dark cream to slightly greenish cream; it has weak anisotropy with rotation tints in shades of pale orange brown to grey and exhibits no internal reflections. Reflectance values of roterbärite in air (R_2, R_1 in %) are: 42.4/43.0 at 470 nm, 45.4/44.4 at 546 nm, 46.8/44.6 at 589 nm and 47.7/44.6 at 650 nm. Eighteen electron-microprobe analyses of roterbärite gave an average composition (in wt%): Pd 18.1 wt%, Bi 35.2 wt%, Cu 10.5 wt%, Se 33.5 wt% and S 2.6 wt%, totalling 99.8 wt% and corresponding to the empirical formula $Pd_{1.01}Cu_{0.98}Bi_{1.00}(Se_{2.53}S_{0.48})_{3.01}$, based on 6 atoms; the average of ten microanalyses on its synthetic analogue is: Pd 17.62 wt%, Cu 10.74 wt%, Bi 33.59 wt% and Se 38.70 wt%, the total of which is 100.65 wt% and corresponds to $Pd_{1.01}Cu_{1.03}Bi_{0.98}Se_{2.98}$. The ideal formula is $PdCuBiSe_3$. The density, calculated on the basis of the empirical formula, is 7.23 g/cm^3. The mineral is orthorhombic, space group $P2_12_12_1$, with a 5.00520(10), b 7.9921(2) Å, c 13.5969(2) Å, V 543.90(2) Å^3 and Z = 4. The crystal structure was solved and refined from the powder X-ray diffraction data of synthetic $PdCuBiSe_3$. Roterbärite crystallizes in the $(Bi,Sb)CuNiS_3$ structure-type, being isostructural with minerals of the lapieite group – i.e., lapieite ($CuNiSbS_3$), mückeite ($CuNiBiS_3$) and lisiguangite ($CuPtBiS_3$). Roterbärite belongs to the vast group of sulfosalts and related compounds (a selenio-salt). The strongest lines in the powder X-ray diffraction pattern of the synthetic $PdCuBiSe_3$ [d in Å (I) (hkl)] are: 3.3593 (97) (103), 3.1226 (100) (120), 3.0434 (75) (121), 2.3894 (39) (105), 1.9210 (70)(223).

Keywords Roterbärite · Synthetic $PdCuBiSe_3$ · Roter Bär mine · Harz Mountains · Germany

Editorial handling: L. Bindi

✉ Anna Vymazalová
anna.vymazalova@geology.cz

[1] Czech Geological Survey, Geologická 6, 152 00 Prague, Czech Republic

[2] Centro de Pesquisa Professor Manoel Teixeira da Costa (CPMTC), Instituto de Geociências, Universidade Federal de Minas Gerais (UFMG), Av. Antônio Carlos 6.627, Belo Horizonte, MG 31270-901, Brazil

[3] Centro de Desenvolvimento da Tecnologia Nuclear (CDTN), Av. Antônio Carlos 6.627, Belo Horizonte, MG 31270-901, Brazil

[4] Technische Universität Clausthal, Adolph-Roemer-Str. 2A, 38678 Clausthal-Zellerfeld, Germany

[5] Department of Earth Sciences, Natural History Museum, Cromwel Road, London SW7 5BD, UK

Introduction

Roterbärite, ideally $PdCuBiSe_3$, was identified at Roter Bär, a former underground mine in the north-eastern part of the St. Andreasberg polymetallic vein district in the Harz Mountains, Germany. Geologically, Roter Bär is a vein-style deposit within a Lower Paleozoic sedimentary sequence underneath a post-Variscan unconformity. The holotype specimen, collected in 1924 by mine geologist Ernst Bock and Prof. Hermann Rose (Hamburg University), represents a selenide-bearing carbonate veinlet that was exposed along a cross adit about 170 m below the surface, the Sieberstollen Bärener Querschlag. Geilmann and Rose (1928) provided the first study of the Roter Bär selenide mineralization.

Cabral et al. (2015) reported an unknown mineral corresponding to $PdCuBiSe_3$, together with gold, mertieite-II and

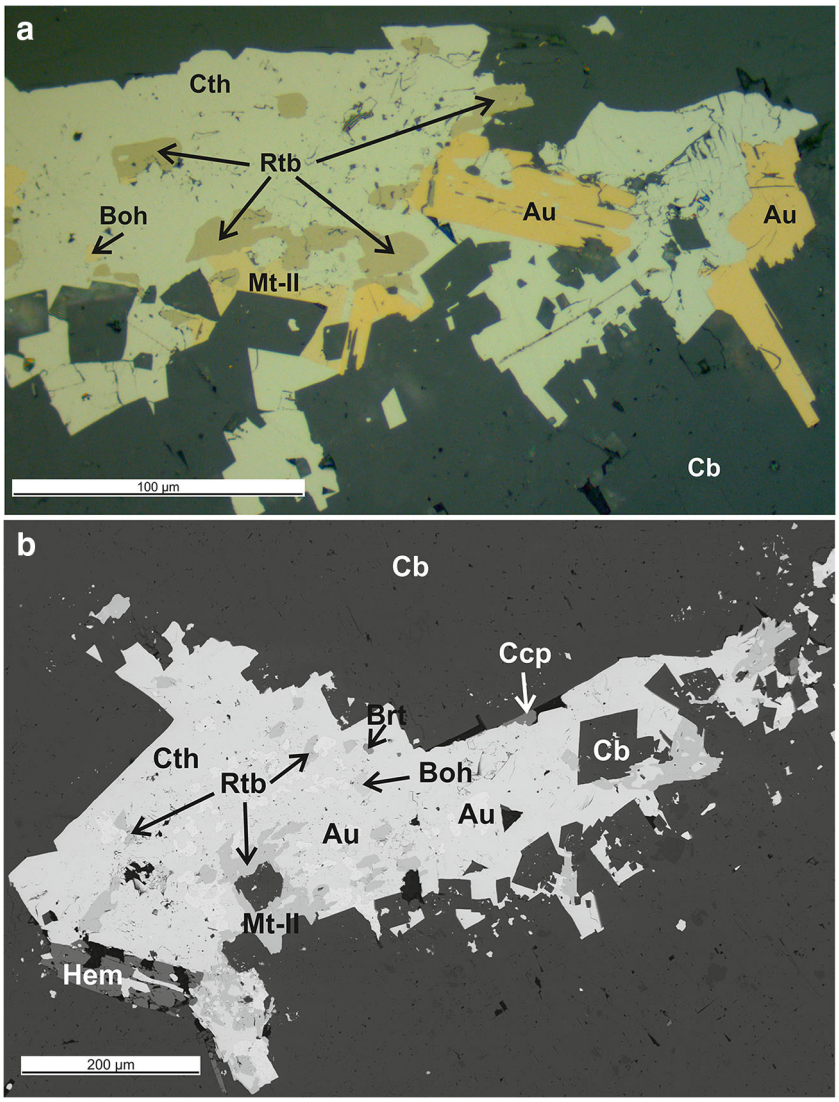

Fig. 1 **a**) Reflected-light photomicrograph of roterbärite (Rtb) inclusions in clausthalite (Cth), in spatial association with gold (Au), bohdanowiczite (Boh) and mertieite-II (Mt-II), in a matrix of vein carbonate (Cb). **b**) Backscattered-electron image of a clausthalite aggregate (Cth) with inclusions of roterbärite (Rtb), gold (Au), bohdanowiczite (Boh), mertieite-II (Mt-II), chalcopyrite (Ccp), baryte (Brt), in spatial association with hematite (Hem) in carbonate (Cb)

bohdanowiczite, occurring in clausthalite–hematite pockets a few millimeters across within a vein-carbonate matrix. The co-existence of roterbärite and bohdanowiczite at Roter Bäre mine suggests a formation temperature of <120 °C, which is the highest stability temperature of hexagonal $AgBiSe_2$ (Wernick 1960), which is the synthetic equivalent of bohdanowiczite. The hematite–selenide–gold association and its geological setting can be reconciled in a scenario involving oxidized brines, carrying metals dissolved from Permo-Triassic red beds, and precipitation of their metal load underneath the post-Variscan unconformity.

The mineral is named after its type locality, the Roter Bär mine, in the Harz Mountains of Germany, for which a location map is given in Cabral et al. (2015). Both mineral and name were approved by the Commission on New Minerals, Nomenclature and Classification (CNMNC) of the International Mineralogical Association (2019–043; Vymazalová et al. 2019). The holotype material of roterbärite, polished thin section, along with its synthetic analogue (Experiment number 53) are deposited in the Mineral Collections of Geosammlung at the Technische Universität Clausthal, Adolph-Roemer-Straße 2A, D-38678 Clausthal-Zellerfeld, Germany. Roterbärite, $PdCuBiSe_3$, belongs to the lapieite group (2.GA.25 of the Nickel–Strunz classification), Strunz and Nickel (2001).

Appearance, physical and optical properties

Roterbärite occurs: (i) as inclusions attaining up to about 50 µm across in clausthalite pockets (Fig. 1); (ii) as isolated grains that are generally less than 10 µm across in the vein carbonate that hosts the clausthalite pockets; (iii) as vein-carbonate-hosted aggregates with either clausthalite or baryte. The aggregates of roterbärite and clausthalite are generally <100 µm across, whereas those of roterbärite and baryte are

Table 1 Reflectance values for roterbärite in comparison with its synthetic analogue

	roterbärite		synthetic analogue	
λ (nm)	R_2 (%)	R_1 (%)	R_2 (%)	R_1 (%)
400	38.8	41.0	39.0	40.0
420	39.6	41.6	39.9	41.0
440	40.7	42.2	41.4	42.0
460	41.8	42.7	42.8	42.9
470	**42.4**	**43.0**	**43.5**	**43.2**
480	42.9	43.3	44.3	43.6
500	43.8	43.8	45.6	44.3
520	44.6	44.2	46.7	44.8
540	45.3	44.4	47.7	45.1
546	**45.4**	**44.4**	**47.8**	**45.1**
560	45.8	44.6	48.3	45.2
580	46.5	44.6	48.6	45.2
589	**46.8**	**44.6**	**48.6**	**45.2**
600	47.0	44.6	48.7	45.2
620	47.4	44.6	48.8	45.2
640	47.6	44.6	48.9	45.1
650	**47.7**	**44.6**	**49.0**	**45.0**
660	47.8	44.6	49.0	45.0
680	48.1	44.6	49.2	44.9
700	48.2	44.7	49.4	44.7

Note: The values required by the Commission on Ore Mineralogy of the International Mineralogical Association are given in bold

<30 μm across. Associated minerals are gold, mertieite-II, bohdanowiczite, clausthalite, hematite, chalcopyrite, baryte, ankerite and dolomite.

Roterbärite is opaque and has a metallic luster. Its color and streak are greyish white and grey, respectively. The mineral density, calculated on the basis of empirical formula and unit-cell volume refined from powder X-ray diffraction (XRD) data, is 7.23 $g.cm^{-3}$.

In reflected light, roterbärite appears dark cream to slightly greenish cream in a strongly colored assemblage where, by comparison, clausthalite appears bluish white, mertieite II appears bright cream and bohdanowiczite, pinkish cream; gold (containg up to 14 wt.% Ag, Cabral et al. 2015) is bright yellow as usual. It is slightly pleochroic in shades of dark cream to slightly greenish cream; it has weak anisotropy with rotation tints in shades of pale orange brown to grey. Reflectance values, measured in air with a WTiC reference material, are listed in Table 1 and plotted in Fig. 2. Reflected-light images of studied samples were taken using a Zeiss Axio Image A2m microscope equipped with a digital camera Axiocam 305 color.

Synthesis of a roterbärite analogue

The grain size of roterbärite is up to 50 μm across, and its inclusion in clausthalite prevents extraction and isolation in an amount suitable for crystallographical and structural investigations. Therefore, a synthetic analogue was prepared for this purpose.

Synthetic $PdCuBiSe_3$ phase was prepared using the evacuated silica-glass-tube method at the Laboratory of Experimental Mineralogy of the Czech Geological Survey in Prague. Palladium (of 99.95 wt% purity), copper (99.999 wt%), bismuth (99.9999 wt%) and selenium (99.999 wt%) were the starting materials for the synthesis.

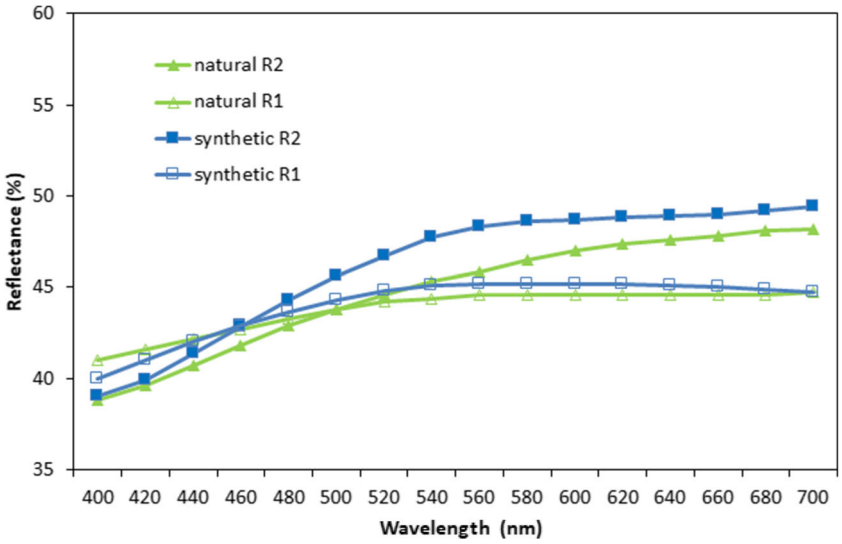

Fig. 2 Reflectance data for roterbärite compared to synthetic $PdCuBiSe_3$ in air. The reflectance values (R %) are plotted versus wavelength λ in nm

Table 2 Main element contents of roterbärite and its synthetic analogue in weight percent (wt%), by EPMA. Further explanation in the main text

element	LLD	roterbärite (n = 18*)			synthetic analogue (n = 10)			nominal
composing elements in weight percent [wt%]								
		average	max	min	average	max	min	stoichiom.
Pd	0.28	18.1	19.0	17.2	17.62	17.95	16.98	17.28
Cu	0.35	10.5	11.0	9.8	10.74	11.46	10.14	10.32
Bi	0.19	35.2	36.6	33.4	33.59	34.26	33.17	33.94
Se	0.14	33.5	37.7	29.6	38.70	38.98	38.30	38.47
S	0.08	2.6	4.7	0.2	–			–
sum		99.80			100.65			100.00
apfu calculated on basis of 6 atoms								
		average			average			stoichiom.
Pd	–	1.01			1.01			1.00
Cu	–	0.98			1.03			1.00
Bi	–	1.00			0.98			1.00
Se	–	2.53			2.98			3.00
S	–	0.48			–			–
$\Sigma_{(Se+S)}$	–	3.01			2.98			3.00
Σ_{metals}	–	2.99			3.02			3.00

* Spot numbers in Table 3 from Cabral et al. (2015), p 654, showing maximum and minimum contents of S. Lead was additionally analyzed for, but it was below the lower limit of detection (LLD) of 0.50 wt%.

Carefully weighted mixture of Pd (0.11614 g), Cu (0.06934 g), Bi (0.22916 g) and Se (0.25852 g) were loaded into the silica-glass tube, tightly fitting silica rod was placed on top of the charge. The evacuated tube with its charge was sealed under oxygen-hydrogen flame and then annealed at 800 °C for 1 day. After cooling by cold-water bath, the charge was ground into powder in acetone using an agate mortar, and thoroughly mixed to homogenize. The pulverized material of synthetic $PdCuBiSe_3$ was again charged into a silica-glass tube, evacuated, sealed and then kept at 200 °C for three months. The experimental product was rapidly quenched in cold water. Phase identity of the synthetic product is elaborated in detail further below.

Chemical composition

The chemical composition of the fine-grained roterbärite was determined on polished thin sections, prepared from original holotype sample material. The sections were polished using diamond pastes of 4, 2, 1 and 0.25 μm in grain size; for electron-backscatter diffraction, colloidal alumina was employed for final polishing. Prior to microanalysis, the polished sections were sputtered with carbon in a Cressington C208 coater to prevent charging.

Electron-probe microanalyses (EPMA) were obtained by wavelength-dispersive X-ray spectrometry (WDS), using a Cameca SX100 instrument at the Technische Universität

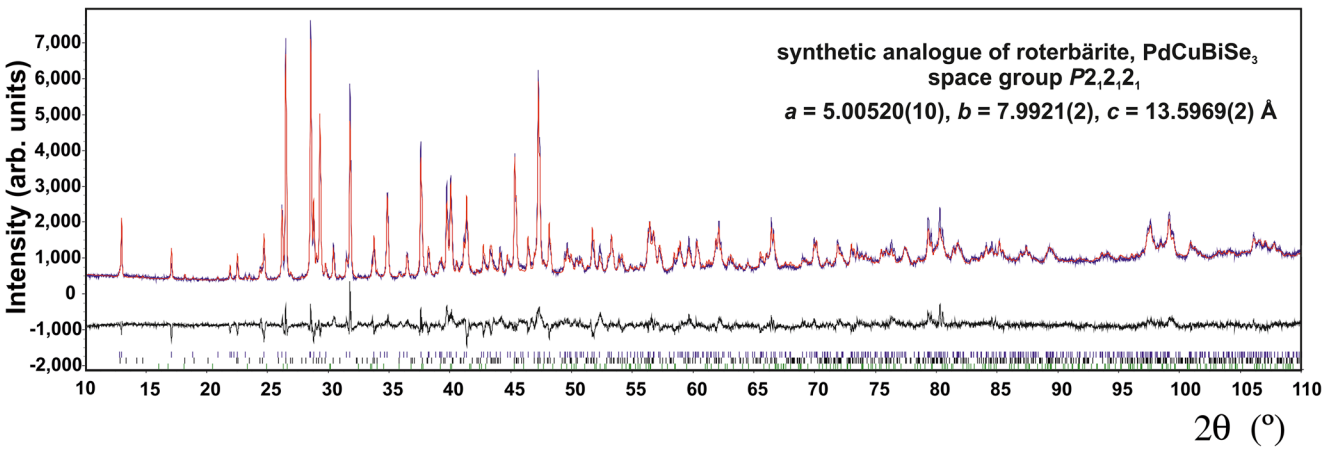

Fig. 3 Final Rietveld fit for synthetic $PdCuBiSe_3$. In addition to the synthetic $PdCuBiSe_3$, the sample contains 6.5 wt% $Cu_{1.78}Bi_{4.74}Se_8$ and about 0.5 wt% PdBi (polarite) as impurities

Table 3 Powder X-ray diffraction data of $PdCuBiSe_3$, the synthetic equivalent of roterbärite. (Cu$K\alpha$ radiation, Bruker D8 Advance, Bragg-Brentano geometry, fixed divergence slit). The five strongest diffractions are highlighted in bold

$I_{(obs)}$	$d_{(obs)}$	$d_{(calc)}$	h	k	l
38	6.7951	6.7984	0	0	2
20	5.1766	5.1783	0	1	2
12	3.9419	3.9425	0	1	3
28	3.5982	3.5988	1	1	2
30	3.3984	3.3992	0	0	4
97	**3.3593**	**3.3596**	**1**	**0**	**3**
100	**3.1226**	**3.1228**	**1**	**2**	**0**
28	3.0975	3.0971	1	1	3
75	**3.0434**	**3.0436**	**1**	**2**	**1**
8	2.9968	2.9974	0	2	3
11	2.8373	2.8378	1	2	2
73	2.8121	2.8120	1	0	4
22	2.6533	2.6526	1	1	4
39	**2.3894**	**2.3895**	**1**	**0**	**5**
29	2.2660	2.2661	0	0	6
37	2.2481	2.2482	0	2	5
25	2.1806	2.1802	0	1	6
9	2.0510	2.0508	1	2	5
8	1.9542	1.9541	2	1	4
70	**1.9210**	**1.9210**	**2**	**2**	**3**
14	1.8874	1.8875	0	1	7
10	1.8344	1.8341	1	2	6
12	1.7662	1.7661	1	1	7
11	1.7174	1.7173	1	4	3
12	1.4930	1.4928	1	2	8

Table 4 Data collection and Rietveld analysis of $PdCuBiSe_3$, the synthetic equivalent of roterbärite

Data collection	
Radiation type, source	X-ray, Cu$K\alpha$
Generator settings	40 kV, 30 mA
Range in 2θ (°)	10–110
Step size (°)	0.01
Crystal data	
Space group	$P2_12_12_1$ (No. 19)
Unit-cell content	$PdCuBiSe_3$, $Z = 4$
Unit-cell parameters (Å)	$a = 5.00520(10)$
	$b = 7.9921(2)$
	$c = 13.5969(2)$
Unit-cell volume (Å^3)	543.90(2)
Rietveld analysis	
No. of reflections	435
No. ofstructural parameters	19
Crystal size (nm)	85(1)
R_{Bragg}	0.051
R_p	0.066
R_{wp}	0.086

Clausthal, Germany. The instrument was operated at 15 kV and 20 nA, with beam diameter of 1 μm, to measure for Pd $L\alpha$, Cu $L\alpha$, Bi $M\alpha$, Se $L\alpha$, and S $K\alpha$, having pure metals for Pd and Cu, Bi_2Se_3 for Bi and Se, and PbS for S as internal reference materials for calibration. No other element was detected by means of energy-dispersive spectrometry (EDS). Microanalytical work on synthetic $PdCuBiSe_3$ was performed with a Cameca SX100 electron-probe micro-analyzer in the wavelength-dispersive mode, the electron beam of which was focused to 1–2 μm. Pure elements were used as reference materials. X-ray lines and operating conditions were as follows: Pd$L\alpha$, Bi$M\alpha$, Cu$K\alpha$, and Se$L\alpha$; an accelerating voltage of 15 kV and a beam current of 10 nA.

Results of eighteen electron-probe microanalyses are summarized in Table 2, together with selected microanalyses from Cabral et al. (2015) for comparison, The empirical formula of roterbärite, calculated on the basis of 6 atoms, is $Pd_{1.01}Cu_{0.98}Bi_{1.00}(Se_{2.53}S_{0.48})_{3.01}$ and $Pd_{1.01}Cu_{1.03}Bi_{0.98}Se_{2.98}$ for its synthetic analogue. The ideal formula of roterbärite is $PdCuBiSe_3$.

X-ray study of synthetic $PdCuBiSe_3$

The synthetic analogue was prepared for X-ray powder diffraction analysis by manual thorough pulverization under acetone in an agate mortar and pestle. To minimize the shape of background in the powder diffraction pattern, the sample was placed on the surface of a flat silicon wafer from acetone suspension and subsequently dried at laboratory temperature.

Powder X-ray diffraction data were collected on synthetic $PdCuBiSe_3$, in Bragg-Brentano geometry of a Bruker D8 Advance powder diffractometer instrument, using Cu$K\alpha$ radiation, 10 mm automatic divergence slit and a Lynx Eye-XE detector. The Ni-β filter placed in the diffracted beam and energy resolution of the detector were used for monochromatisation of the X-rays. The data were collected in the 2θ angular range from 10 to 110 °, in 0.01 °2θ steps, with 1.2 s counting time per step, and overall scan time of 3 h 49 m 56 s. Powder diffraction pattern (Fig. 3) was processed with Diffrac. Eva 4.1 proprietary Bruker software using the PDF-2 database (ICDD 2018). Indexed line positions and relative intensities I/I_0 are summarized in Table 3.

The initial structure model from the Rietveld refinement of synthetic $PdCuBiSe_3$ was derived from the isostructural $PdCuBiS_3$ synthetic phase, which crystallizes in the $P2_12_12_1$ space group (Laufek et al. 2019). The sulfur positions were replaced by selenium positions and such a model was refined from the powder X-ray diffraction data by the Rietveld method. The program Topas5 was used for the refinement (Bruker 2014). The Rietveld method involved the refinement of unit-cell parameters, crystal-structure coordinates, isotropic size and isotropic displacement parameters. In order to reduce

Table 5 Atomic positions (space group $P2_12_12_1$) for the synthetic equivalent of roterbärite, $PdCuBiSe_3$

Atom	Wyckoff letter	*x*	*y*	*z*	B_{iso}	*BVS**
Bi	4*a*	0.9149(5)	0.3820(4)	0.13100(11)	0.39(7)	3.27(3)
Pd	4*a*	0.5018(9)	0.13181(10)	0.2520(10)	0.39(7)	2.17(3)
Cu	4*a*	0.9644(10)	0.3814(11)	0.4392(4)	1.6(2)	0.98(1)
Se1	4*a*	0.7342(11)	0.1234(11)	0.4107(3)	0.39(7)	2.17(3)
Se2	4*a*	0.2506(10)	0.3841(11)	0.2941(3)	0.39(7)	2.20(2)
Se3	4*a*	0.2826(10)	0.1348(10)	0.0894(3)	0.39(7)	2.05(3)

The isotropic displacement parameter B_{iso} was constrained to be equal for Bi, Pd and Se atoms during the refinement. *Bond-valence sums

correlations of refined parameters, the atomic coordinates were consecutively refined following the guidelines of McCusker et al. (1999). The isotropic displacement parameters were constrained to be equal for all atoms except Cu in the structure. In total, 30 parameters were refined. The background was determined by means of a Chebychev polynomial of the fifth order. The final Rietveld plot is shown in Fig. 3, details of data collection and basic crystallographic data are in Table 4. Table 5 lists atomic coordinates and bond-valence sums.

The crystal structure of synthetic analogue of roterbärite contains three independent metal positions (Cu, Pd and Bi) and three Se positions (Fig. 4). The Cu site displays a strongly deformed tetrahedral coordination with 2 + 2 bonding scheme with two shorter (2.394–2.404 Å) and two longer (2.438–2.448 Å) Cu-Se bonds (Table 6). These distances are comparable to those observed in synthetic $CuFeSe_2$ (2.419 and 2.424 Å) by Delgado et al. (1992). Slightly longer Cu-Se distances (2.449–2.527 Å) were observed in nearly regular [$CuSe_4$] tetrahedra in grudmannite, $CuBiSe_2$ (Förster et al. 2016), Table 6. Palladium atoms show square-planar coordination as is typical of the $4d^8$ electron configuration of Pd^{2+}. The Pd-Se distances range from 2.418(8) to 2.468(13) Å, comparable to those found in jaguéite, $Ag_2Pd_3Se_4$ (Topa et al. 2006) and tischendorfite, $Pd_8Hg_3Se_9$ (Laufek et al. 2014). The [$PdSe_4$] squares are almost perfectly planar; the Se(1)-Pd-Se(3) and Se(2)-Pd-Se(2) angles are 178.8(2)° and 178.5(3)°, respectively. Palladium atoms show two additional Bi distances at 3.296(8) and 3.313(8) Å, oriented perpendicularly to the [$PdSe_4$] squares (Fig. 4). Bismuth atoms are surrounded by four Se atoms in the 3 + 1 bonding scheme with distances ranging from 2.669(8) to 3.072(4)Å. Their coordination is further completed by two Pd atoms at distances of 3.296(8) and 3.313(8) Å forming the [BiS_4Pd_2] dipyramid. There are no short Pd–Pd, Cu–Pd or Cu–Cu distances (<3.7 Å).

The crystal structure of synthetic analogue of roterbärite forms a three-dimensional framework composed of corner-sharing [$CuSe_4$] deformed tetrahedra and [$PdSe_4$] squares. Within this framework, the [$CuSe_4$] deformed tetrahedra share opposing corners and form *zigzag* chains running along the **a** axis. The [$PdSe_4$] squares

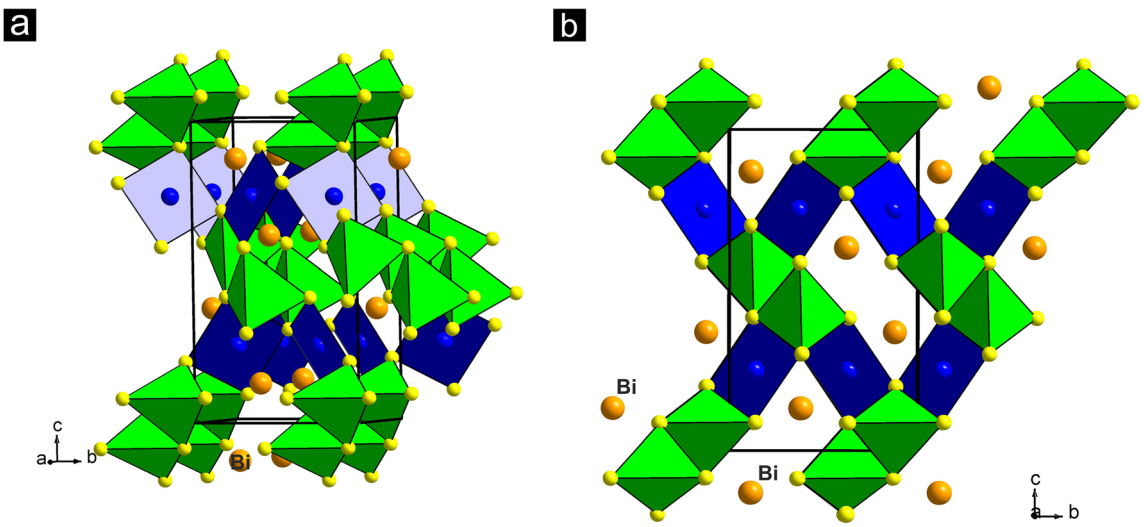

Fig. 4 Polyhedral representation of the roterbärite crystal structure: (**a**) inclined view; (**b**) view along the *a* axis. The [$CuSe_4$] tetrahedra and [$PdSe_4$] squares are highlighted; Bi atoms are light orange

Table 6 Selected bond distances (Å) in the crystal structure of synthetic equivalent of roterbärite, $PdCuBiSe_3$

Cu	Se(1)	2.394(11)	Bi	Se(1)	2.669(8)
	Se(3)	2.404(10)		Se(3)	2.758(7)
	Se(2)	2.438(7)		Se(2)	2.782(5)
	Se(1)	2.448(7)		Se(3)	3.072(4)
				Pd	3.296(8)
Pd	Se(2)	2.418(8)		Pd	3.313(8)
	Se(2)	2.444(8)			
	Se(1)	2.452(12)			
	Se(3)	2.468(13)			
	Bi	3.296(8)			
	Bi	3.313(8)			

are connected via opposing vertices and make up chains oriented along the *b* direction (Fig. 5). Both chains share common Se vertices of the respective coordination polyhedra. Bismuth atoms occupy channels running along the **a** axis.

Equivalence of roterbärite and its synthetic analogue $PdCuBiSe_3$

A TESCAN Mira 3GMU scanning electron microscope, combined with a NordlysNano electron backscattered diffraction (EBSD) detector, Oxford Instruments, was used for EBSD measurements. The natural sample was prepared for investigation by etching the mechanically polished surface with colloidal silica (OP-U) for 30 min to reduce the surface damage. The EBSD measurements and data processing were carried out using a proprietary computer program AZtec HKL (Oxford Instruments). The solid angles calculated from EBSD patterns were compared with a structural model match containing eight reflectors to index the patterns. The EBSD patterns, also known as Kikuchi patterns, were obtained from roterbärite, totalling fifty-five measurements on different spots on roterbärite. These measurements were found to match the patterns generated from our refined structural model for synthetic $PdCuBiSe_3$ (Fig. 6). Values of the mean angular deviation, MAD – i.e., goodness of fit – between the calculated and measured Kikuchi bands, vary between 0.26 ° and 0.54 °. Such values reveal a very good match. Values of MAD that are less than 1 ° are considered an acceptable fit (HKL Technology 2004).

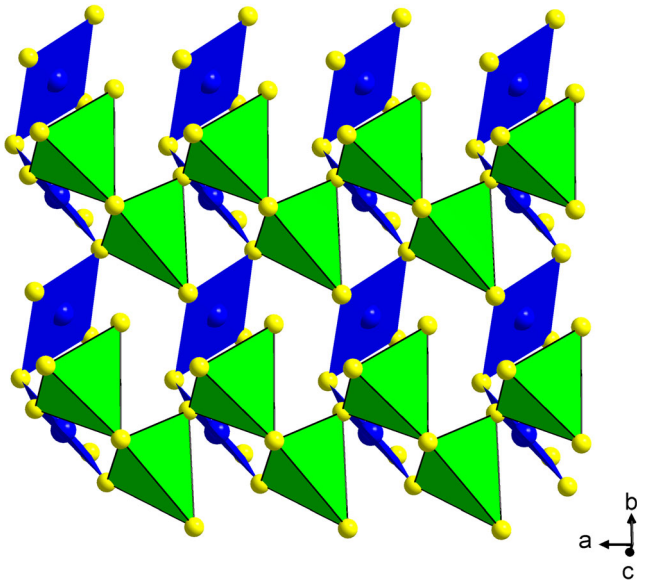

Fig. 5 Chains of [$PdSe_4$] squares and [$CuSe_4$] tetrahedra in the crystal structure of roterbärite

Conclusion

Roterbärite crystallizes in the (Bi,Sb)$CuNiS_3$ structure-type and is isostructural with minerals of the lapieite group – i.e., lapieite ($CuNiSbS_3$), mückeite ($CuNiBiS_3$) and lisiguangite ($CuPtBiS_3$). Another member of the lapieite group, malyshevite ($CuPdBiS_3$), shows *Pnam* symmetry and a different unit cell (Chernikov et al. 2006). Its crystal structure has not been hitherto determined. The lapiete group belongs to the wide group of sulfosalts (Moëlo et al. 2008). Minerals

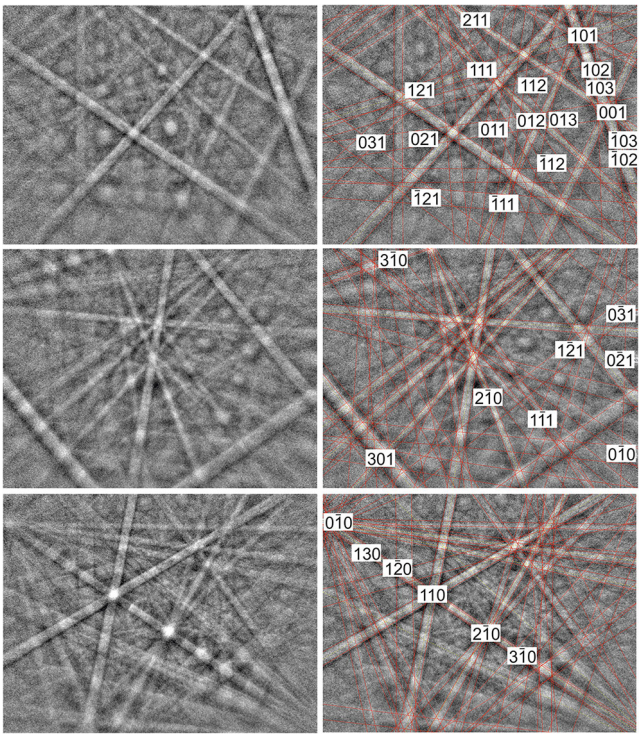

Fig. 6 EBSD images of roterbärite in grains of different orientations; in the right column the Kikuchi bands are indexed

Table 7 Minerals of the Lapieite group, comparative data and the comparison with the bournonite group

Mineral name	Formula	Crystal stucture		*a* (Å)	*b* (Å)	*c* (Å)	*V* (Å^3)	Z	ρ (g·cm^{-3})	Reference
Lapieite group										
lapieite	$CuNiSbS_3$	Orthorhombic	$P2_12_12_1$	7.422	12.508	4.900	454.9	4	4.966	Harris et al. 1984
mückeite	$CuNiBiS_3$	Orthorhombic	$P2_12_12_1$	7.514	12.557	4.880	459.7	4	5.88	Bente et al. 1990; Schnorrer-Köhler et al. 1989
lisiguangite	$CuPtBiS_3$	Orthorhombic	$P2_12_12_1$	7.685	12.882	4.9243	487.5	4	7.42	Yu et al. 2009
malyshevite	$CuPdBiS_3$	Orthorhombic	*Pnam*	7.541	6.4823	11.522	563.2	4	6.025	*Chernikov et al. 2006
synthetic	$CuPdBiS_3$	Orthorhombic	$P2_12_12_1$	4.8847	7.5885	12.8646	476.86	4	6.62	Laufek et al. 2019
roterbärite	$PdCuBiSe_3$	Orthorhombic	$P2_12_12_1$	5.0052	7.9921	13.5969	543.9	4	7.23	this study
Bournonite group										
bournonite	$PbCuSbS_3$	Orthorhombic	$Pn2_{1m}$	8.153	8.692	7.793	552.26	4	5.83	Edenharter et al. 1970
seligmannite	$PbCuAsS_3$	Orthorhombic	$Pn2_1m$	8.076	8.737	7.634	538.66	4	5.38	Edenharter et al. 1970
součekite	$PbCuBi(S,Se)_3$	Orthorhombic	$Pn2_1m$	8.15	8.49	8.08	559.08	4	7.50	Čech and Vavřín 1979
cerromojonite	$CuPbBiSe_3$	Orthorhombic	$Pn2_1m$	8.202	8.741	8.029	575.7	4	7.035	Förster et al. 2018

*Crystal structure not determined

belonging to the lapieite group are summarized in Table 7. Roterbärite is chemically related to cerromojonite, $PbCuBiSe_3$ (Table 7). However, cerromojonite has the bournonite-type structure (Förster et al. 2018), and hence it is structurally different from roterbärite.

The EBSD study, chemical identity and optical properties confirm the equivalence of the natural and synthetic materials and, consequently, legitimate the use of the synthetic phase for the complete characterization of roterbärite.

Acknowledgements The authors acknowledge Ritsuro Miyawaki, the Chairman of the Commission on New Minerals, Nomenclature and Classification of the International Mineralogical Association, and its members for their thoughtful comments on the data submitted to the commission. Reviews by Yves Moëlo and Louis J. Cabri as well as the editorial comments by associate editor Luca Bindi and the chief editor Maarten A.T.M. Broekmans are sincerely appreciated. This work was supported by the Grant Agency of the Czech Republic (project 18-15390S to AV). C.J. Stanley acknowledges Natural Environment Research Council grant NE/M010848/1 Tellurium and Selenium Cycling and Supply.

References

Bente K, Doering T, Edenharter A, Kupcik V, Steins M, Wendschuh-Josties M (1990) Structure of the new mineral mückeite, $BiCuNiS_3$. Acta Cryst C46:127–128

Bruker AXS (2014) Topas 5, computing program. Bruker AXS GmbH, Karlsruhe, Germany

Cabral AR, Lieβmann W, Lehmann B (2015) Gold and palladium minerals (including empirical $PdCuBiSe_3$) from the former Roter Bär mine, St. Andreasberg, Harz Mountains, Germany: a result of low-temperature, oxidising fluid overprint. Mineral Petrol 109:649–657

Čech F, Vavřín I (1979) Součekite, $CuPbBi(S,Se)_3$, a new mineral of the bournonite group. N Jahrb Mineral Monat:289–295

Chernikov AA, Chistyakova NI, Uvarkina OM, Dubinchuk VT, Rassulov VA, Polekhovsky YS (2006) Malyshevite $PdBiCuS_3$ – a new mineral from Srednyaya Padma deposit in southern Karelia. New Data on Minerals 41:14–17

Delgado JM, Diaz de Delgado G, Quintero M, Woolley JC (1992) The crystal structure of copper iron selenide, CuFeSe2. Mater Res Bull 27:367–373

Edenharter A, Nowacki W, Takéuchi Y (1970) Verfeinerung der Kristallstruktur von Bournonit [(SbS) |Cu Pb Pb] und von Seligmannit [(AsS) |Cu Pb Pb]*. Zeitschrift für Kristallographie 131:397–417

Förster H-J, Bindi L, Stanley CJ (2016) Grundmannite, $CuBiSe_2$, the se-analogue of emplectite, a new mineral from the El Dragón mine, Potosí, Bolivia. Eur J Mineral 28:467–477

Förster H-J, Bindi L, Grundmann G, Stanley CJ (2018) Cerromojonite, $CuPbBiSe_3$, from El Dragón (Bolivia): a new member of the bournonite group. Minerals 8:420

Geilmann W, Rose H (1928) Ein neues Selenerzvorkommen bei St. Andreasberg im Harz. N Jahrb Mineral Geol Paläont Abh A 57: 785–816

Harris DC, Roberts AC, Thorpe RI, Jonasson IR, Criddle AJ (1984) Lapieite $CuNiSbS_3$, a new mineral species from the Yukon territory. Can Mineral 22:561–564

HKL Technology (2004) Channel 5. HKL–Technology A/S, Hobro, Denmark

ICDD (2018) PDF-2 2018. International Centre for Diffraction Data. Newtown Square, PA, USA

Laufek F, Vymazalová A, Drábek M, Navrátil J, Drahokoupil J (2014) Synthesis and crystal structure of tischendorfite $Pd_8Hg_3Se_9$. Eur J Mineral 25:157–162

Laufek F, Vymazalová A, Navrátil J, Chareev DA, Plášil J (2019) Crystal structure and transport properties of $CuPdBiS_3$. J Alloy Comp 792: 983–987

McCusker LB, von Dreele RB, Cox DE, Louër D, Scardi P (1999) Rietveld refinement guidelines. J Appl Crystallogr 32:36–50

Moëlo Y, Makovicky E, Mozgova NN, Jambor JL, Cook N, Pring A, Paar W, Nickel EH, Graeser S, Karup-Møller S, Balic-Žunic T,

Mumme WG, Vurro F, Topa D, Bindi L, Bente K, Shimizu M (2008) Sulfosalt systematics: a review. Report of the sulfosalt subcommittee of the IMA Commission on ore mineralogy. Eur J mineral 20: 7-46 of copper iron selenide, $CuFeSe_2$. Mater Res Bull 27: 367–373

Schnorrer-Köhler G, Neumann U, Doering T (1989) Mückeite, $CuNiBiS_3$, a new mineral from the Grüne Au mine, Schutzbach/Siegerland. N Jahrb Mineral Monat 5:193–200

Strunz H, Nickel EH (2001) Strunz mineralogical tables. E. Schweizerbartsche Verlagsbuchhandlung, Stuttgart, Germany, 870 pp

Topa D, Makovicky E, Balić-Žunić T (2006) The crystal structures of jaguéite, $Cu_2Pd_3Se_4$, and chrisstanleyite, $Ag_2Pd_3Se_4$. Can Mineral 44:497–505

Vymazalová A, Cabral AR, Laufek F, Lieβmann W, Stanley CJ, Lehmann B (2019) Roterbärite, IMA2019-043. CNMNC newsletter no. 51; mineral mag 83. https://doi.org/10.1180/mgm.2019.58

Wernick JH (1960) Constitution of the $AgSbS_2$–PbS, $AgBiS_2$–PbS, and $AgBiS_2$–$AgBiSe_2$ systems. Am Mineral 45:591–598

Yu Z, Cheng F, Ma H (2009) Lisiguangite, $CuPtBiS_3$, a new platinum-group mineral from the Yanshan Mountains, Hebei, China. Acta Geol Sin 83:238–244